High speed train-induced ground motion and interaction with structures

P. Galvín, J. Domínguez *

Escuela Superior de Ingenieros, Universidad de Sevilla, Camino de los Descubrimientos s/n, 41092 Sevilla, Spain

Abstract

A general numerical model for the analysis of soil motion due to high-speed train passage and effects on nearby surface and underground structures is presented in this paper. Soil, ballast and structures are represented using a 3-D time domain boundary element approach. Material damping has been included in the time domain formulation. Equilibrium and compatibility between soil and underground or surface structures is established in a rigorous manner in order to take into account soil-structure interaction. In contrast to other existing approaches, effects on a particular structure and the influence of non-uniform soil conditions along the track can be evaluated. Numerical results are obtained for different situations and some of them are compared with existing experimental records. The experimental values are to a large extent reproduced by the present numerical approach. Ballast influence and effects of high-speed train passage on a concrete underpass structure are analyzed.

Key words: High-speed train, Transient dynamic, BEM, Experimental validation

1 Introduction

Many new high speed train (HST) lines are being constructed in Europe, Asia and the USA. The growing interest in the analysis of train-induced in recent years calls for additional studies to be conducted in this area. Problems such as train vibrations, soil free field vibrations produced by train traffic, and dynamic effects on structures situated near the track, are much more important

* Corresponding author. Tel.: +34 954487293; fax: +34 954487295.
Email address: jose@us.es (J. Domínguez).

in the case of high speed trains than for conventional ones. A thorough analysis of these effects is required in order to ensure security and comfort in the trains and to avoid eventual problems for nearby constructions which may be affected by vibrations induced by waves transmitted through the soil. Particularly serious would be situations in which the train speed may be higher than that of the surface waves in the underlying soil. Such a possibility was completely unthinkable for conventional trains but it is now something that should be taken into account when high speed trains operate at locations with soft soils or underground discontinuities that may result in relatively low surface wave speed. Worthy of note here is the record speed of 574.8 km/h (159.7 m/s) set by a French train travelling between Paris and Strasburg in April 2007.

The study of these problems requires employing comprehensive models that can take into account significant factors related to the characteristics of the train, the track, and the local soil properties. Nearby structures should also be modelled in case where the effects on these structures are being analyzed. The final objective of this paper is to make gains in being able to accurately predict soil wave propagation due to the passage of HST and to forecast vibrations that will affect existing structures and those to be constructed.

Different analytical, semi-analytical or numerical methods for the analysis of HST-induced vibrations have been developed in recent years. One of the important aspects of the problem is modelling the force transmitted by the train to the soil through the rail beam and the sleepers. Particularly noteworthy was the model presented by Krylov [1,2] and Krylov and Fergurson [3] during the nineties. In this model, they consider a quasi-static force transmitted by the sleepers and combine it with Green's functions of a half-space in order to represent the wave propagation through the soil. More advance models of similar type were presented in [4–6].

Several papers have dealt with train track dynamics with ground interaction in the last decade. Dieterman and Metrikine [7,8] used a beam model on an equivalent one-dimensional spring system for the half-space. The model was replaced by a stratum by Metrikine and Popp [9]. Focusing on the track system, some other papers take into account the fact that rails are supported discretely by the ground and that sleepers have a significant inertia effect on the rails. Metrikine and Popp [10] and Vostroukhov and Metrikine [11] considered these factors by taking a general solution for the differential equation. Takemiya and Bian [12] make an extension of [10], by including a layered soil analysis and use a discrete Kelvin model for the sleepers' complex frequency-dependent stiffness.

Different authors have also presented approaches for the analysis of soil induced vibrations due to moving loads (road or train traffic) using Green's

functions for a layered half-space. Most of them are based on the so-called two-and-a-half-dimensional fundamental solution, obtained by Tadeu and Kausel [13], combined with a boundary element (BE) discretization. Some of these works were presented by Clouteau et al [14], Lombaert and Degrande [15,16], Lombaert et al. [17,18], Degrande et al. [19], Degrande [20], and Degrande and Schillemans [21].

Andersen and Nielsen [22] presented a boundary element method (BEM) formulation for the analysis of the response of an elastic half-space to a moving surface force. They used a frequency domain full space Green's function formulated in a frame of reference and obtained the time-domain solution by means of Fourier transformation. A time-domain BEM using a fundamental solution in a frame of reference was proposed by Chouw and Pflanz [23].

Numerical procedures for the analysis of ground vibrations produced by HST based on the combination of BEM and FEM have also been presented by several authors [24,25]. Auersch [26] has recently presented a rather comprehensive model using a combined FEM-BEM model for soil and track and a multi-body model for the vehicle, to calculate the dynamic compliance. Sheng et al. [27] also use a FEM/BEM approach for the analysis of ground vibration produced by trains. These papers and some others [28–30] are based on the idea that the ground and structures such as tunnels and tracks, are homogeneous in the track direction. This assumption, which simplifies the analysis to a large extent, is realistic for the study of free field motion and vehicle vibrations in many parts of a line; however, the analysis of ground vibrations in zones with local discontinuities in the soil properties or the effects on structures such as underpasses, buildings and auxiliary structures around the track, require of a fully three-dimensional model. Situations with important dynamic soil-structure interaction effects also required of a comprehensive model where the interaction is taken into account by coupling both domains rigorously.

In this paper, a general and fully three-dimensional BEM model for the analysis of the soil motion and the effects of HST passage on nearby surface and underground structures is presented. Soil, ballast and structures are represented using 3-D time domain BEM. Structures can also be represented by a FE model. A full-space fundamental solution is used in combination with quadratic BE. Special attention is given to stabilization algorithms and element subdivision to improve efficiency, stability and accuracy. Internal material damping is introduced in the BE formulation in a simple and efficient manner. The formulation presented is more general than other existing approaches. It permits full coupling between the soil and nearby structures; it is able to consider embankment, ballast and other local effects, as well as coupling with structures that brake uniformity of the geometry along the track direction. In the following, the time domain BEM formulation is summarized first. Second, internal damping is introduced in the formulation. Third, an

analysis of the ground motion induced on a homogeneous half-space by the HST passage is carried out. Fourth, the effects of ballast and embankment geometry are studied, and the obtained results are validated by comparison with those obtained by other authors and existing experimental records. Last of all, the effect of HST passage on an underpass structure is analyzed. Motion at different points and loads on the structure are obtained. Effects of HST passage on different types of structures, while taking 3-D and soil-structure interaction effects into rigorous consideration, will be presented in an upcoming paper. To the authors' knowledge, no previous studies include the employment of a fully numerical model in the analysis of HST passage effects on local structures, taking dynamic soil-structure interaction rigorously into account. Some of the basic numerical aspects of the BE approach presented in this paper were tested in a previous paper by the same authors [31] using much simpler preliminary problems.

2 Time domain BEM for 3-D problems

The three dimensional time domain BE formulation for transient problems is very briefly summarized in this section. This topic is more thoroughly addressed in Domínguez [32] and Marrero and Domínguez [33].

The integral representation of the displacement u at a point i on the boundary of an elastic body, at time t with zero body forces and zero initial conditions can be written as [32]:

$$\begin{aligned} c_{lk}^{i} u_{k}^{i}(\mathbf{x}^{i}, t) = & \int_{0}^{t^{+}} \int_{\Gamma} u_{lk}(\mathbf{x}, t-\tau; \mathbf{x}^{i}) p_{k}(\mathbf{x}, \tau) d\Gamma(\mathbf{x}) d\tau \\ & - \int_{0}^{t^{+}} \int_{\Gamma} p_{lk}(\mathbf{x}, t-\tau; \mathbf{x}^{i}) u_{k}(\mathbf{x}, \tau) d\Gamma(\mathbf{x}) d\tau \end{aligned} \tag{1}$$

where u_k and p_k stand for the k component of the displacement and traction, respectively; $u_{lk}(\mathbf{x}, t-\tau; \mathbf{x}^i)$ and $p_{lk}(\mathbf{x}, t-\tau; \mathbf{x}^i)$ are the fundamental solution displacement and traction tensors, respectively, at point $\mathbf{x}$ due to a point load at $\mathbf{x}^i$. The coefficient c_{lk}^i depends only on the boundary geometry at point i. Displacements and tractions over the boundary are approximated from their nodal values at each time step u_k^{mj} and p_k^{mj}, the space interpolation functions $\phi^j(r)$ and $\psi^j(r)$, and the time interpolation functions $\eta^m(\tau)$ and $\mu^m(\tau)$.

After interpolation of the boundary variables Equation (1) becomes

$$c_{lk}^{i}u_{k}^{ni} = \sum_{m=1}^{n}\sum_{j=1}^{Q}\left[\left\{\int_{\Gamma_j}\Big[\int_{\Delta t_m} u_{lk}\mu^{m}d\tau\Big]\psi^{j}d\Gamma\right\}p_{k}^{mj} - \left\{\int_{\Gamma_j}\Big[\int_{\Delta t_m} p_{lk}\eta^{m}d\tau\Big]\phi^{j}d\Gamma\right\}u_{k}^{mj}\right] \tag{2}$$

where Q is the total number of boundary nodes and Γ_j are the elements to which node j belongs. The integrals of $u_{lk}\mu^m$ and $p_{lk}\eta^m$ for each time step are usually called U_{lk}^{nm} and P_{lk}^{nm}, respectively.

Thus, equation (2) becomes

$$c_{lk}^{i}u_{k}^{ni} = \sum_{m=1}^{n}\sum_{j=1}^{Q}\left[\left\{\int_{\Gamma_j} U_{lk}^{nm}\psi^{j}d\Gamma\right\}p_{k}^{mj} - \left\{\int_{\Gamma_j} P_{lk}^{nm}\phi^{j}d\Gamma\right\}u_{k}^{mj}\right] \tag{3}$$

which in a more compact form can be written as

$$c_{lk}^{i}u_{k}^{ni} = \sum_{m=1}^{n}\sum_{j=1}^{Q}\left[G_{lk}^{nmij}p_{k}^{mj} - \hat{H}_{lk}^{nmij}p_{k}^{mj}\right] \tag{4}$$

Once the independent term c_{lk}^{i} is included in the system matrix, the integral representation for point i at time $t = n\Delta t$ becomes

$$\sum_{m=1}^{n}\sum_{j=1}^{Q} H_{lk}^{nmij}u_{k}^{mj} = \sum_{m=1}^{n}\sum_{j=1}^{Q} G_{lk}^{nmij}p_{k}^{mj} \tag{5}$$

and the system of equations for all the boundary nodes at time $t = n\Delta t$ can be written in matrix form as

$$\sum_{m=1}^{n}\mathbf{H}^{nm}\mathbf{u}^{m} = \sum_{m=1}^{n}\mathbf{G}^{nm}\mathbf{p}^{m} \tag{6}$$

Once the boundary conditions are applied, Equation (6) yields a system of equations which can be solved step-by-step to obtain the time variation of the boundary unknowns.

Piecewise constant time interpolation functions $\mu^m(\tau)$ are used for tractions and piecewise linear functions $\eta^m(\tau)$ for displacements. The time integrals in Equation (2) can be evaluated analytically without much difficulty. In the present paper, nine node rectangular and six node triangular quadratic elements are used. Each side of the element is divided into equal parts in the natural coordinates domain yielding an element subdivision. The spatial integration extends only to those subdivisions whose mid-points are under the effects of the fundamental solution waves according to the causality condition of each term of the fundamental solution.

Ensuring that the stepping procedure stable is an important issue in time domain BEM. To do so an approach based on the idea of using a linear combination of equations for several time steps in order to advance one step, is applied in the present paper. A constant velocity is assumed at each time step to predict traction and displacement values in the time step ahead of that being computed. Details of this stabilization approach can be found in [33].

3 Internal soil damping

It is well known that wave amplitudes decrease as they propagate in solids due to material internal damping. Material damping effects in soil motions due to high-speed trains have been experimentally observed by different authors (Madshus and Kaynia [34], Degrande and Schillemans [21], Degrande [35], Auersch [26]).

Including viscous material damping in a frequency domain BEM formulation is simple [32]. Using complex valued shear modulus of the type $\mu(1+2\xi i)$, where ξ is the viscous damping coefficient, or $\mu(1+\zeta i)$ where ζ is the hysteretic damping coefficient ($\zeta = 2\xi$), internal damping is taken into account in a very simple and straightforward way. However, to consider internal damping in time domain BEM formulations is not that simple. Several authors [36,37] have proposed different approaches where Laplace or another transform type would permit the introduction of internal damping at a high computational cost. Jin et al. [38] proposed a simple approach for 2D problems with a dominant frequency in the system response. The approach, based on the idea that periodic oscillators present a constant amplitude logarithmic decrement per period, is extended here to 3-D problems and used for the analysis of soil motion induced by high-speed train passage. The basic idea is rather simple: a damping term is introduced in the boundary integral equation as

$$\begin{aligned} c^i_{lk} u^i_k(\mathbf{x}^i,t) = &\int_0^{t^+} \left[\int_\Gamma u_{lk}(\mathbf{x}, t-\tau; \mathbf{x}^i) p_k(\mathbf{x},\tau) d\Gamma(\mathbf{x}) \right] \exp\left(-2\pi\xi(t-\tau)/T\right) d\tau \\ &- \int_0^{t^+} \left[\int_\Gamma p_{lk}(\mathbf{x}, t-\tau; \mathbf{x}^i) u_k(\mathbf{x},\tau) d\Gamma(\mathbf{x}) \right] \exp\left(-2\pi\xi(t-\tau)/T\right) d\tau \end{aligned} \tag{7}$$

where the damping term is determined from the viscous damping coefficient ξ or the hysteretic coefficient $\zeta = 2\xi$, and the dominant vibration period T in the response. Once the integral equation is discretized one obtains the following equation for each time step

$$\mathbf{H}^{nn}\mathbf{u}^u = \mathbf{G}^{nn}\mathbf{p}^u + \sum_{m=1}^{n-1} \left(\mathbf{G}^{nm}\mathbf{p}^m - \mathbf{H}^{nm}\mathbf{u}^m\right) \exp\left(-2\pi\xi(n-m)\Delta t/T\right) \tag{8}$$

where the right hand side term derived from previous steps is damped by an exponential coefficient with linearly increasing exponent, as time goes on.

It should also be mentioned here that the material damping term included in Equations 7 and 8 is consistent with that proposed by Barkan [39] in his classical work where an attenuation law depending on the distance r from the source and the dominant period T

$$u^{\xi}(r) = u^{\xi}(r^0)\left(\frac{r}{r^0}\right)^{-n} \exp\left(\frac{-2\pi\xi(r-r^0)/c}{T}\right) \tag{9}$$

is assumed. Note that $(r/r_0)^{-n}$ corresponds to radiation damping, which in the BEM case is included in the exact fundamental solution.

Results obtained with the model represented by Equations (7) and (8) have been shown to be accurate, as compared to known solutions and experimental results for situations simpler than train-induced ground vibration problems [31]. Even though the present damping model is based on an attenuation law for vibrations with a known period, good results can be obtained using a reference dominant period. In particular, for high-speed train induced vibrations one can use a dominant frequency in the range 40 Hz to 80 Hz depending on the train speed. These values correspond to the intermediate range, containing the relatively high peaks of the experimental frequency spectra shown in Figures 10-12.

4 Homogeneous half-space motion due to train passage

A problem of soil vibrations induced by a high-speed train passage will be studied next. The train is considered to be a set of axle loads travelling at constant speed and the soil a uniform viscoelastic half space.

4.1 Axle load distribution and near field discretization

The load is assumed to be transmitted to the soil by each couple of wheels through the sleepers according to the load distribution proposed by Krylov [40]. He obtained a quasi-static load distribution pattern among several sleepers that transmit the load of an axle. In this model, the track is represented as a beam on a Winkler foundation. The model does not incorporate some sources of vibration such as rail roughness, wheel flats and parametric excitation. The distribution depends on the rail beam stiffness ($EI = 12.76 \times 10^6$ Nm^2 is assumed for two rail beams), the ballast stiffness ($k_s = 250$ MPa is

assumed) and the mass per unit length including both of the rails and the sleepers ($m = 620$ kg/m is assumed). The values for the track have been taken from Degrande [20].

The rail beam vertical displacement w is obtained from the solution of the differential equation

$$EI\frac{\partial^4 w}{\partial y^4} + m\frac{\partial^2 w}{\partial t^2} + k_s w = T\delta(y - vt) \tag{10}$$

where T is the axle load.

The solution of Equation (10) is given by [40]:

$$w(y-vt) = \frac{T}{8EI\beta^3\delta}\exp(-\beta\delta|y-vt|)\left(\cos\beta\eta(y-vt)+\frac{\delta}{\eta}\sin\beta\eta|y-vt|\right) \tag{11}$$

where $\beta = (k_s/EI)^{0.25}$, $\delta = [1 - (v/c_{min})^2]^{0.25}$, $\eta = [1 + (v/c_{min})^2]^{0.25}$ and $c_{min} = (4k_sEI/m^2)^{0.25}$ is the wave propagation velocity along the beam.

The load $P(t)$ transmitted to the soil by one of the sleepers located at $y = 0$ is:

$$P(t) = \frac{T}{N_{eff}^{st}}\frac{w(vt)}{w_{max}^{st}} \tag{12}$$

where N_{eff}^{st} is the number of sleepers supporting the load in the case that all the sleepers had the maximum rail beam deflection. It can be seen from this equation that each sleeper transmits a fraction of the axle load T proportional to the track deflection at time t.

Figure 1.(a) shows the load transmitted to the soil by one sleeper when a unit axle load travels at a speed of $v = 315$ km/h. The load distribution depends to a certain extent on the load velocity. The frequency content corresponding to this load variation with time is shown in Figure 1.(b).

Prior to any train passage analysis, and in order to asses the most appropriate BE mesh for the soil surface, a very refined mesh is first assumed for a rather short patch on the soil surface along the track. It includes (Figure 2.(a)) the length corresponding to 36 sleepers and a width of 21.28 m, 960 being the total number of elements. The surface under each sleeper is discretized into six rectangular elements and so is the surface between two sleepers (Figure 3.(a)). The rest of the elements are also quadrilateral with size increasing with distance to the track. The mesh in Figure 2.(a) is very dense and, therefore, able to accurately represent the soil behaviour near the loaded area; but, it is not long enough to properly represent the effect of a load that is travelling from far away and whose influence on a given observation point starts long before the load is over this discretized area. It would be necessary to make it

several times longer, but this would give way to an extremely large number of elements.

A less dense mesh is tested to represent the soil around the track. The new mesh for the same surface is shown in Figure 2.(b). The smallest elements in this case are 1.2 m $\times$ 1.25 m rectangles arranged in a way such that two elements represent the area corresponding to two sleepers and two intermediate areas. A row of 5 nodes is on the mid line of each sleeper (Figure 3.(b)). To compare the two meshes in figures 2.(a) and 2.(b), a load of 15×10^4 N travelling at 315 km/h from one end of the mesh to the other is assumed. The time step size is $\Delta t = 0.003$ s. In the first case (Figures 2.(a) and 3.(a)), the pressure corresponding to each sleeper according to Krylov's distribution is applied to the 39 nodes on each sleeper. In the second (Figures 2.(b) and 3.(b)) this traction is applied to 5 nodes on the same sleepers. It should be taken account that in this second case, as the shape functions extend over the complete element, the area between two sleepers would also be loaded. An equivalent load is given by the relationship between the total load under the sleepers according to Krylov's distribution in the first mesh, and the total load that would be transmitted to the soil in the simplified BE model where tractions are prescribed at the corresponding nodes. This relation depends on Krylov's distribution, which in turn depends on the rail beam-ballast-soil properties and the load velocity. In the case considered, with a load speed 315 km/h, the relation is 0.345. Taking into account this correction for the second mesh, surface displacements are evaluated using both meshes. The soil is assumed to be a homogeneous elastic half-space with shear modulus $\mu = 18.5 \times 10^6$ N/m^2; Poisson's ratio, $\nu = 0.3$ and density, $\rho = 1850$ kg/m^3. Vertical and cross displacement components obtained at points on the mid cross section located at several distances from the track axis show that both meshes give almost identical soil surface displacements. This fact and results for other preliminary tests for different speed values lead to the conclusion that elements such as those pertaining to the coarse mesh can be used to represent the soil surface near the track.

4.2 Homogeneous half-space surface motion

The analysis of the soil vibrations induced by a high speed train on an homogeneous viscoelastic half-space is now carried out using the BE mesh of Figure 4 which has a total length of 86.4 m, a width of 25 m, and elements for the track zone of the same type as those in Figure 2.(b). The train is represented by an array of loads corresponding to the axles location and load values of trains Alstom (Thalys) as shown in Figure 5 and Table 1.

In 1997, Degrande and coworkers [20,21,35] made a set of experimental mea-

surements for this train just before the inauguration of the high-speed train track between Brussels and Paris. These valuable data, presented and discussed by Degrande and Schillemans [21] and Degrande [35], will be used in this paper for comparison with numerical results obtained using the proposed BE technique.

The train characteristics, and the rail and sleeper properties, are as given in references [21,20]. The soil is assumed to be a uniform viscoelastic half-space with shear-wave velocity $c_s = 100$ m/s, a Poisson's ratio $\nu = 0.3$ and a mass density $\rho = 1850$ kg/m^3. These soil properties coincide with those assumed by Degrande [20] for a top layer of thickness $d = 1.4$ m; taking into account a measured value at the actual site of 80 m/s and assuming that the soil under the track had been made stiffer by stabilization before construction. This 100 m/s value assumption for the top layer is based on measured values and experience. Numerical studies carried out by the authors for a point load travelling at constant speed, within the train speed range considered, on the surface of a stratum with the properties reported by Degrande [20] ($h_1 = 1.4$ m, $c_{s1} = 100$ m/s; $h_2 = 1.9$ m, $c_{s2} = 133$ m/s; and bedrock $h_3 = \infty$, $c_{s3} = 226$ m/s), show that surface motion is almost identical to that of a uniform half-space with $c_s = 100$ m/s. A viscous damping ratio $\xi = 0.03$ was estimated in [20]; however, Degrande [20] indicates that this value may underestimate damping at the top layer. Because of that, a viscous damping ratio $\xi = 0.04$ has been assumed in the present analysis. Some additional discussion on the soil properties will be carried out in the following sub-section. The assumed reference dominant frequency for the attenuation law is train speed dependent and it falls within the intermediate frequency range (40 Hz $< f_d <$ 80 Hz). In particular, that corresponding to half of the sleeper passing frequency has been chosen in this study (for instance, $f_d = 59$ Hz for $v = 256$ km/h).

Train speed values $v = 315$ km/h, $v = 300$ km/h, $v = 271$ km/h and $v = 256$ km/h were assumed for the BE numerical analysis. Experimentally recorded values are available for these train speeds. The load transmitted to one of the sleepers by a unit axle load is obtained from Equations (11) and (12). Its time variation and frequency content for a load speed $v = 315$ km/h was shown in Figure 1. The load time history and frequency content for the Alstom (Thalys) train, obtained by superposition, is shown in Figure 6. The free-field time response for a train passage was obtained using the 3-D time domain technique presented above using the discretization shown in Figure 4 and a time step $\Delta t = 0.003$ s. The response to a single axle load, producing a surface load at each sleeper of the type shown in Figure 1, was obtained for each velocity. Then the response for the complete train was obtained by superposition.

It should be mentioned here that to validate the mesh in Figure 4, the problem of a point load travelling at constant speed on the surface of half-space

without track was studied first using the same mesh. A good agreement between numerical and analytical solution was obtained for the same velocities and properties of the present study. Results of that experiment can be seen in [31]. The size of the elements used in Figure 4 discretization is small enough to represent the soil surface motion of the problem at hand for an axle load at the speeds of interest. It should be borne in mind that the frequency content is as shown in Figure 1 and that a 10×10 element subdivision is used to carry out numerical integration over the boundary elements. The time step used in the analysis is short enough to produce accurate BE results [33] for one axle load and to preserve accuracy in the superposition process. Previous BE analysis of soil vibration problems show that a mesh several times as wide as the loading zone is enough to obtain accurate results in the area around the loading zone [32]. In the present study, a mesh width of 25 m was chosen in order to be able to measure soil surface displacements up to 10 m from the track axis. An accurate representation of the soil surface displacements at larger distances would require a wider mesh.

Displacement records at any point on the boundary element mesh are obtained from the numerical analysis. Points on the cross-symmetry axis of the discretized zone are taken as a reference. Figure 7 corresponds to the time records of the vertical component velocity at a surface point located at 4 m from the track axis and the four speed values mentioned above. Experimental data and time-domain BE computed values are shown in the figure for the four train speed values. The same type of representation can be seen for points at 6 m and 8 m from the track axis in Figures 8 and 9, respectively. A high frequency pass filter with a roll-off termination frequency $f_t = 2.5$ Hz and a cut-off frequency $f_c = 3.0$ Hz has been applied. This filter was used in order to compare numerical results with the experimental values reported by Degrande [20] who used the filter to compute velocity values from recorded acceleration data.

Frequency spectra for the BEM numerical results were obtained using the Fourier transform. Frequency spectra are shown in Figures 10, 11 and 12 for distances of 4 m, 6 m and 8 m to the track axis, respectively. It can be observed from these figures that numerical results are dominated by bogie and axle passage frequency (low frequency). This part of the numerical results spectra corresponds closely to the experimental results spectra. However, the intermediate frequency content of the experimental results spectra, corresponding to wheel and rail irregularities, are not shown by the time records and frequency spectra of the numerical results as they are not included in the load model.

A good representation of damping is important for the numerical calculation of ground vibrations. Radiation damping plays a key role in the system motion. This damping mechanism is very accurately represented in the BEM since it is exactly included in the fundamental solution. Attenuation law in Equations

(7) and (8) and the assumed damping ratio take the material damping effect into consideration. To study this effect, a parametric analysis is carried out. Computed PPV as a function of distance to the track for an Alstom (Thalys) train passage are represented in Figures 13.(a), 13.(b) and 13.(c) for three different train speeds: subsonic ($v = 300$ km/h), transonic ($v = 350$ km/h), and supersonic ($v = 500$ km/h), respectively. In each case three different damping ratios where considered $\xi = 0.02$, $\xi = 0.04$ and $\xi = 0.06$. It can be seen from Figure 13 that soil vibration PPV is higher for transonic train speed than for supersonic and subsonic train speed. The PPV decreases more rapidly with the distance for higher amplitude soil vibrations. When the material damping is very high ($\xi = 0.06$) the soil PPV is rather small for all the distance range represented and depends very little on the train speed.

Several additional comments can be made regarding to the results shown in Figures 7 to 13:

(1) In all cases, the time length of the main perturbation, the normal peak particle velocity (PPV) values and the dominant frequency corresponding to bogies and axle passage are accurately represented in the BE solution. There is good agreement between numerical results and experimental measures.
(2) The PPV values are almost independent of the train speed for moving speed values lower than the surface wave velocity. However, dynamic ground response increases rapidly when the train speed is close to the "critical velocity" (c_R) as shown in Figure 13. For speeds higher than c_R the amplitude decreases. Obviously, the frequency content of the soil motion shifts to higher values with increasing train speed since the excitation frequencies increase.
(3) The present time domain boundary element approach can be employed to properly the time history of soil surface motion at a significant area around the track, including the attenuation effects, for different train speeds.
(4) The most significant difference between experimental and BE computed values is that experimental values contain intermediate frequency peaks, superimposed to the dominant bogie and axle passage peaks, which are not obtained in the numerical solution. These peaks are due to excitation mechanisms, such as rail or wheel irregularities, which are not included in Krylov's load model. Nevertheless, the PPV and the most significant frequencies are accurately represented by the present BE approach.

5 Ballast and embankment effects

Ballast and train-track embankment geometry and properties play an important role on the soil motion due to high-speed train passage. Their effects can be evaluated by representing the actual ballast and embankment geometry and properties using the BE technique presented in this paper. Only one has to take into account regions with different properties and their actual geometry. In order to asses this effect, two different numerical experiments carried out by the authors will be analyzed next.

First, a simple geometry and loading situation is studied in order to validate the proposed approach. Consider an homogeneous soil and a 0.8 m thick embankment with a geometry as shown in Figure 14. This problem was studied by Adam et al. [29] using 2-D and 3-D approaches. In the 3-D case, those authors discretized a 48 m $\times$ 16 m wide area using space constant boundary elements (4800 elements for the half-space and 1320 for the embankment). In the present work, an area of 48m$\times$32m is discretized using 768 quadratic elements for the half-space and 768 quadratic elements for the embankment. Following Adam et al. [29] and in order to use their results for comparison, the train track load is represented by two impulse line loads with unit amplitude (10^3 N/m) that last for 0.02 s which are applied where the two beam rails are located. Mass density $\rho = 2000$ kg/m^3 and a Poisson's ratio $\nu = 1/3$ are assumed to be identical for embankment and half-space.

Two cases are evaluated for comparison purposes. In Case 1 the S-wave velocity is the same for embankment and half-space ($c_s = 250$ m/s); in Case 2, $c_s = 250$ m/s for the embankment and $c_s = 400$ m/s for the half-space. Soil surface vertical displacements at two points A and B are represented in Figures 15.(a) and 15.(b). A is located under the load (the rail beam line) and B on the half-space surface 6 m from the rail beam. Figures 15.(a) and 15.(b) show computed vertical displacement time history for Case 1 and Case 2, respectively. Results are compared with those obtained by Adam et al. [29]. There is very good agreement between both sets of results. Figures 15.(a) and 15.(b) show a vertical displacement under the load line (point A) that increases with time as the load is being applied (0 s$\leq t <$ 0.02 s). Once the load is withdrawn, vertical displacement under the load line goes to zero as it does for a quasistatic load ($t >$ 0.02 s). Straight line segments in Figures 15.(a) and 15.(b) are due to the time stepping process. As pointed out in [29], apart from the little kinks due to wave scattering at the embankment edges, the soil response for Case 1 is very similar to that of a half-space since the only difference is in the surface profile. A positive maximum of the vertical displacement corresponding to the first S-wave arrival time is observed in Figure 15.(a) for the point at 6 m from the load (point B). After that time, vertical displacement at point B decreases to the minimum value when the effect of the load withdrawal is

noticed at that point (Rayleigh waves from the nearest loading point). The vertical displacement peak values at both points are smaller in Case 2 than in Case 1 as could be expected for a stiffer half-space.

A similar study to that presented before for the Alstom (Thalys) train travelling on the surface of a half-space at different speeds, will be carried out next. The soil instead of being an homogeneous half-space, has a ballast layer 1 m thick which is wide enough for two rail tracks as shown in Figure 16. The soil and ballast are discretized using quadratic boundary elements as shown in the figure. The discretized area is 86.4 m long and 37 m wide. The soil under the ballast is an homogeneous viscoelastic half-space whose mass density, Poisson's ratio and damping coefficient are the same as they were in section 4.2. A shear wave velocity $c_s = 80$ m/s is now assumed. This value was obtained from experimental measurements in [20] for the upper soil layer of the actual site where soil vibrations due to this type of train were measured. The ballast has the same mass density and Poisson's ratio as the half-space. It is stiffer than the underlying soil with a shear wave velocity $c_s = 200$ m/s and a viscous damping coefficient $\xi = 0.03$.

The same train with its corresponding load values and relative position as in the half-space analysis (section 4.2) are assumed in this case. Krylov's pressure distribution on the sleepers and train velocities $v = 315$ km/h, $v = 300$ km/h, $v = 271$ km/h and $v = 256$ km/h are also assumed. A time step $\Delta t = 0.003$ s has also been chosen in this case. The computed time history for the vertical displacement at a point 4 m from the track axis is shown in Figure 17 for the four velocities considered. Time histories for vertical displacements at points 6 m and 8 m from the track axis are shown in Figures 18 and 19, respectively. Some comments can be made on the present results as compared to those previously obtained for an equivalent stiffer half-space without ballast and the experimentally measured results. Both were shown in Figures 7 to 9.

(1) Numerical results obtained for a $c_s = 200$ m/s ballast layer on a $c_s = 80$ m/s homogeneous half-space are very similar to the experimentally measured values and to those obtained for a homogeneous half-space with and S-wave velocity $c_s = 100$ m/s, as can be seen by comparison of results in Figures 17 to 19 with those in Figures 7 to 9.
(2) A $c_s = 80$ m/s half-space (without ballast) has significantly larger peak values of the soil surface velocities than a $c_s = 100$ m/s half-space. The ballast layer reduces the amplitude of soil surface motion making the response of a $c_s = 80$ m/s half-space with ballast similar to that of a $c_s = 100$ m/s half-space without ballast.
(3) A good representation of the ballast geometry and properties is required for practical studies since its effect on the system response is significant.
(4) The ballast effect could be considered using equivalent properties for the soil; however, it is not easy to estimate values for those equivalent

properties.

(5) A good knowledge of the actual soil properties is required. More in situ measurements of actual high-speed track sites soil properties and soil motion due to high-speed train passage are needed.

6 Dynamic interaction with a concrete underpass structure

One of the important things to be analyzed in the project of high-speed train lines is the dynamic effects on surface and underground structures next to the track. The present BE model allows for a realistic representation of these effects taking into account in a rigorous manner dynamic soil-structure interaction. Soil and structure are included in the same 3-D model and full interaction is considered. To show the capabilities of the approach a practical engineering problem will be studied. The soil motion and the HST effects on a concrete underpass when the train passes at 300 km/h speed are studied. The geometry of the problem and BE discretization for soil and structure are shown in Figure 20. The train passes along an embankment on a uniform half-space. Both half-space and embankment have the same properties: shear-wave velocity $c_s = 100$ m/s; Poisson's ratio $\nu = 0.3$; density $\rho = 1850$ kg/m^3 and viscous damping ratio $\xi = 0.02$. The underpass is a concrete plate type structure with the geometry shown in Figure 20. The concrete is assumed to be a uniform linear elastic material with the following properties: shear modulus $\mu = 0.8 \times 10^{10}$ N/m^2; Poisson's ratio, $\nu = 0.2$ and density, $\rho = 2500$ kg/m^3. Both soil and concrete regions are discretized using quadrilateral and triangular quadratic BE. Equilibrium and displacement compatibility is established for nodes on the soil-concrete interfaces. The full model is analyzed using the step by step BE approach presented above. A 15×10^4 N load due to an axle travelling at 300 km/h is considered first. The load is applied, as in the previous case, using Krylov's load distribution over a group of sleepers under the axle. The subgrade stiffness variation due to the underpass structure has been taken into account to evaluate Krylov's load distribution when the axle passes over the underpass. To do so a numerical evaluation of the static stiffness on this transition zone was carried out. A combination of axle loads is considered to represent an Alstom (Thalys) HST (see Fig. 5) travelling at the same speed as the axle load.

Soil surface displacements in the vertical direction Z due to a 15×10^4 N axle load travelling at 300 km/h are represented for three instants of time in Figure 21. The coordinates origin is located at the point of the underpass half-space surface located on the two planes of symmetry of the problem. The three instants $t = 0.267$ s, $t = 0.537$ s and $t = 0.804$ s correspond to distances X=-22.45 m, X=0.05 m and X=22.30 m, respectively. It can be seen from the figures how the influence of the underpass on the soil surface displacement

is small for $t = 0.267$ s and $t = 0.804$ s. Vertical displacements are almost symmetric and their values are almost the same as for greater distances to the underpass. At $t = 0.537$ s the load is over the underpass and, as compared to the other two cases, the Z displacements values under the load and its vicinity are smaller due to the stiffening effect of the concrete plate located just under the loaded surface.

Figure 22 shows vertical displacements at three half-space surface reference points for the train passage. The three points are shown in Figure 20 as A1, A2 and A3. Their distances to the track axis is 11.5 m and their distance to the plane of symmetry is 23.4 m, 3.6 m and 0 m, respectively. The bogie passage effect can be seen at the three locations. It should be noted that the half-space surface motion at point A1 ($X = -23.4$ m) is almost the same as for points with larger values of X. The maximum displacements of the three points shown, take place at point A2 ($X = -3.6$ m) due to the load transmitted to the soil surface through the concrete walls, whereas point A3 ($X = 0$ m) at the plane of symmetry take intermediate values. In any case, displacements at the half-space surface are much smaller that those at embankment point closer to the track.

Vertical displacements at points B of the embankment at distance $Y = 3.5$ m from the track axis are shown in Figure 23. Values for three points, B1, B2 and B3 at distances 23.4 m, 3.6 m and 0 m, respectively, are shown. The peak displacement values due to the train passage are of one order of magnitude larger than those for the soil surface and decrease very significantly when the point is over the under-pass structure due to its stiffening effect.

Traction values at the underpass deck due to the HST passage are also directly obtained from the model. The time history for two different points C and D of the deck cross track axis of symmetry are shown in Figure 24. Point C is the centre point of the deck (see Figure 20) and point D is on the deck external boundary. As expected, tractions take their maximum values under the sleepers zone and decrease towards the deck external boundary.

Additional numerical results for displacements and tractions on the underpass deck corresponding to different load velocities can be found in [41].

7 Conclusions

A three-dimensional time domain boundary element formulation for viscoelastic solids has been applied to the analysis of soil motion due to high-speed train passage. A decaying law, that takes into account the internal soil material damping has been included in the formulation which is more general

than previous boundary element formulations and allows for a realistic representation of the problem. As compared to frequency domain formulations, the present BE formulation allows for the consideration of coupling with nearby structures that may have a non-linear behaviour. When compared to formulations based on direct integration of half-space Green's functions, the present BE formulation has the added advantage of being able to consider the actual geometry, embankment and ballast effects, and other local effects. As compared to 2.5-D solutions the present formulation can take into account local soil discontinuities, underground constructions such as underpasses, and coupling with nearby structures that brake the uniformity of the geometry along the track line. The present approach is limited by the required computational time for large meshes. Nevertheless, the translation property in space and time of the fundamental solution together with large parts of the soil surface mesh which are uniform and repeat themselves along the track direction allow for development of numerical algorithms that significantly reduce the computational time and increase the model extension. Those computational advantages have not been used in the studies presented in this paper. All the numerical examples presented in this paper have been run using a laptop computer.

Some of the conclusions drawn from the computed numerical results for the particular situations for which there are in situ measurements of soil surface motion due to high-speed train passage are:

(1) The actually measured motion at different distances from the track and different train speed values, are rather accurately reproduced by the present numerical approach. The velocity peak values are accurately evaluated. The model should be improved in order to take into account intermediate frequency motions excited by rail and wheel roughness.
(2) Ballast layers have a significant influence on the system response. They should be considered in the model.
(3) A half-space with equivalent properties may be used to represent soil and ballast effects; however, a prior assessment of the properties of this half-space is difficult. They can be evaluated by comparative analysis of certain simple preliminary problems studied using the actual geometry and properties of soil and ballast, and the equivalent half-space properties.

This paper is intended to develop a general numerical model for the analysis of soil vibrations due to high-speed train passage and their effects on nearby structures. The influence of a concrete underpass structure on the soil motion and the loads on the structure produced by the train passage have been studied. To the authors' knowledge there is not any previous fully 3-D numerical model for the analysis of HST-induced vibrations and their effects on nearby structures, while taking dynamic soil-structure interaction into account.

8 Acknowledgements

The authors would like to thank the group of researchers from the University of Leuven for the valuable experimental data available on their web page. Our thanks are extended as well to the JSV reviewers and editor for their valuable comments that have certainly improved the paper. This research is financed by the Ministerio de Educación y Ciencia of Spain under the research project BIA2004-03955-C02-01 and by the Ministerio de Fomento of Spain under the research project "Evaluación de efectos dinámicos del ferrocarril". The financial support is gratefully acknowledged.

References

[1] Krylov V. On the theory of railway-induced ground vibrations. Journal de Physique IV 1994; **4**: 769-772.

[2] Krylov V. Generation of ground vibrations by superfast trains. Applied Acoustics 1995; **44**: 149-164.

[3] Krylov V. Ferguson C. Recent progress in the theory of railway-generated ground vibrations. Acustica - Acta Acustica 1998; **84**: 78-90.

[4] Knothe K. Wu Y. Receptance behaviour of railway track and subgrade. Archive of Applied Machanics 1998; **68**: 457-470.

[5] Van den Broeck P. De Roeck G. Dynamic behaviour of railway track on layered media. Proceedings of the 3rd European Conference on Structural Dynamics: Eurodyn' 96, Balkema, Rotterdam, 1996, pp. 1083-1089.

[6] Van den Broeck P. De Roeck G. The vertical receptance of track including soil-structure interaction. Proceedings of the 4th European Conference on Structural Dynamics: Eurodyn' 99, Balkema, Rotterdam, 1999, pp. 837-842.

[7] Dieterman HA. Metrikine AV. The equivalent stiffness of a halfspace interacting with a beam. Critical velocities of a moving load along the beam. European Journal of Mechanics, A/Solids 1996; **15**: 67-90.

[8] Dieterman HA. Metrikine AV. Steady-state displacements of a beam on an elastic half-space due to a uniformly moving constant load. European Journal of Mechanics, A/Solids 1997; **6**: 295-306.

[9] Metrikine AV. Popp K. Steady-state vibrations of an elastic beam on a visco-elastic layer under moving load. Archive of Applied Mechanics 2000; **70**: 399-408.

[10] Metrikine AV. Popp K. Vibration of a periodically supported beam on an elastic half-space. European Journal of Mechanics, A/Solids 1999; **18**: 679-701.

[11] Vostroukhov AV. Metrikine AV. Periodically supported beam on a visco-elastic layer as a model for dynamic analysis of a high-speed railway track. International Journal of Solids and Structures 2003; **40**: 5723-5752.

[12] Takemiya H. Bian X. Substructure simulation of inhomogeneous track and layered ground dynamic interaction under train passage. Journal of Engineering Mechanics 2005; **131**: 699-711.

[13] Tadeu A. Kausel E. Green's function for two-and-a-half-dimensional elastodynamic problems. Journal of Engineering Mechanics 2000; **126**: 1093-1097.

[14] Clouteau D. Degrande G. Lombaert G. Numerical modelling of traffic induced vibrations. Meccanica 2001; **36**: 401-420.

[15] Lombaert G. Degrande G. Experimental validation of a numerical prediction model for free field traffic induced vibrations by in situ experiments. Soil Dynamics and Earthquake Engineering 2001; **21**: 485-497.

[16] Lombaert G. Degrande G. The experimental validation of a numerical model for the prediction of the vibrations in the free field produced by road traffic. Journal of Sound and Vibration 2003; **262**: 309-331.

[17] Lombaert G. Degrande G. Clouteau D. Numerical modelling of the free field traffic-induced vibrations. Soil Dynamics and Earthquake Engineering 2000; **19**: 473-488.

[18] Lombaert G. Degrande G. Kogut J. François S. The experimental validation of a numerical model for the prediction of railway induced vibrations. Journal of Sound and Vibration 2006; **297**: 512-535.

[19] Degrande G. De Roeck G. Van dn Broeck P. Smeulders D. Wave propagation in layered dry, satured and unsatured poroelastic media. International Journal of Solids and Structures 1998; **35**: 4753-4778.

[20] Degrande G. Free field vibrations during the passage of a high speed train: experimental results and numerical predictions. In: Krylov V, editor. Noise and vibration from high-speed trains. London: Thomas Telford Publishing, 2001.

[21] Degrande G. Schillemans L. Free field vibrations during the passage of a Thalys HST at variable speed. Journal of Sound and Vibration 2001; **247**: 131-144.

[22] Andersen L. Nielsen SRK. Boundary element analysis of the steady-state response of an elastic half-space to a moving force on its surface. Engineering Analysis with Boundary Elements 2003; **27**: 23-38.

[23] Chouw N. Pflanz G. Reduction of structural vibrations due to moving load. In: Chouw & Schmid, editors. Wave 2000. Balkema, Rotterdam, 2000.

[24] Takemiya H. Ground vibrations alongside tracks induced by high-speed trains: prediction and mitigation, in Noise and Vibration from High-Speed Trains, Krylov VV. (ed), Thomas Telford Publishing; 2001.

[25] Takemiya H. Kojima M. Substructure simulation of inhomogeneous track and layered ground dynamic interaction under train passage. Proceedings of the Ninth International Conference on Civil and Structural Engineering Computing, Egmond-aan-Zee, Netherlands, September 2003.

[26] Auersch L. The excitation of ground vibration by rail traffic: theory of vehicle-track-soil interaction and measurements of high-speed lines. Journal of Sound and Vibration 2005; **284**: 103-132.

[27] Sheng X. Jones CJC. Thompson DJ. Prediction of ground vibration from trains using the wavenumber finite and boundary element methods. Journal of Sound and Vibration 2006; **293**: 575-586.

[28] Jones CJC. Sheng X. Petyt M. Simulations of ground vibrations from a moving harmonic load on a railway track. Journal of Sound and Vibration 2000; **231**: 739-751.

[29] Adam M Pflanz G. Schmid G. Two- and three-dimensional modelling of half-space and train-track-embankment under dynamic loading. Soil Dynamics and Earthquake Engineering 2000; **19**: 559-573.

[30] Karlström A. Boström A. An analytical model for train-induced ground vibrations from railways. Journal of Sound and Vibration 2006; **292**: 221-241.

[31] Galvín P. Domínguez J. Analysis of ground motion due to moving surface loads induced by high-speed trains. Engineering analysis with boundary elements 2007; : In press.

[32] Domínguez J. Boundary elements in dynamics. Southampton, Boston, London, New York: Computational Mechanics Publications and Elsevier Applied Science; 1993.

[33] Marrero M. Domínguez J. Numerical behavior of time domain BEM for three-dimensional transient elastodynamic problems. Engineering analysis with boundary elements 2002; **27**: 39-48.

[34] Madshus C. Kaynia AM. High-Speed Railway Lines On Soft Ground: Dynamic Behaviour At Critical Train Speed. Journal of Sound and Vibration 2000; **231**: 689-701.

[35] Degrande G. Free field vibration measurements during the passage of a Thalys high speed train. Department of Civil Engineering, K.U.Leuven, Internal report BWM-2000-06, 2000.

[36] Wolf JP. Darbre GR. Time-domain boundary element method in visco-elasticity with application to a spherical cavity. Soil Dynamics and Earthquake Engineering 1986; **5**: 138-148.

[37] Gaul L. Schanz M. Dynamics of viscoelastic solids by boundary element approaches in time domain. European Journal of Mechanics A/Solids 1994; **13**: 43-59.

[38] Jin F. Pekau OA. Zhang CH. A 2-D time domain boundary element method with damping. International Journal for Numerical Methods in Engineering 2001; **51**: 647-661.

[39] Barkan DD. Dynamics of Bases and Foundations. New York: McGraw-Hill; 1962.

[40] Krylov V. Effects of track properties on ground vibrations generated by high-speed trains. Acustica-Acta Acustica 1998; **84**: 78-90.

[41] Galvín P. Numerical and experimental study of ground vibrations induced by high speed train passage and effects on structures (in Spanish). PhD Thesis, Universidad de Sevilla, Spain, 2007.

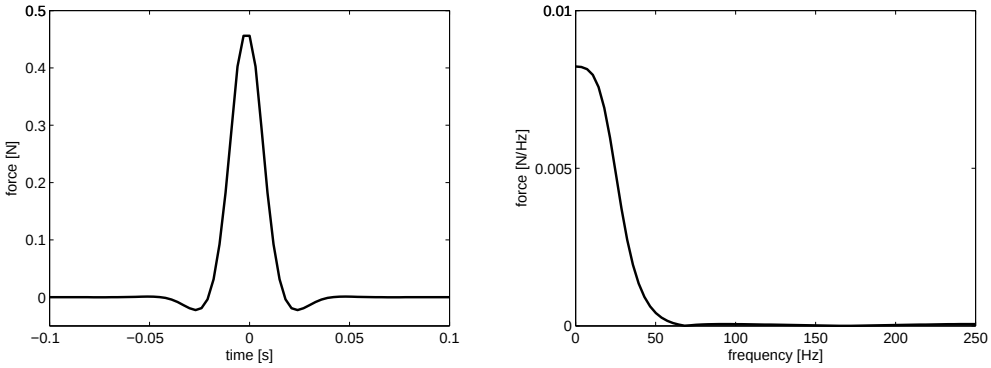

(a) (b)

Fig. 1. Force transmitted by a single sleeper when a unit axle load moves with speed v along the track: (a) Time history (b) Frequency content.

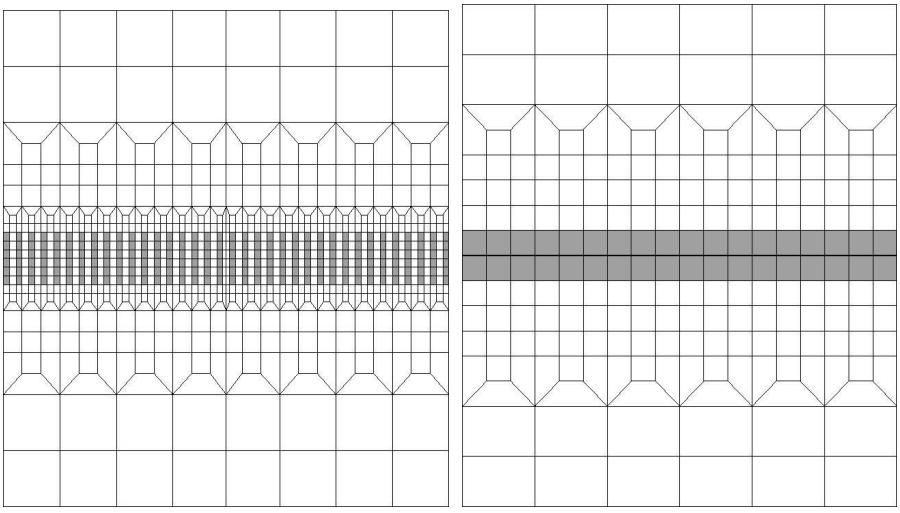

(a) (b)

Fig. 2. Discretization of the surface around the track for a length equivalent to 36 sleepers.

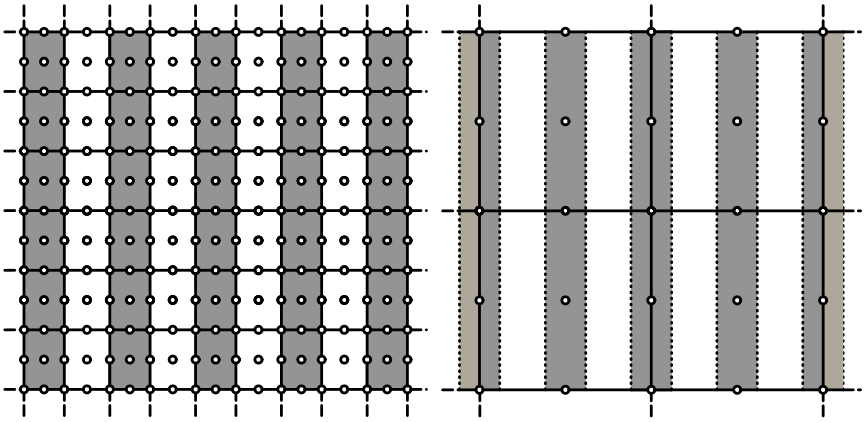

Fig. 3. BE discretization of the sleeper zone

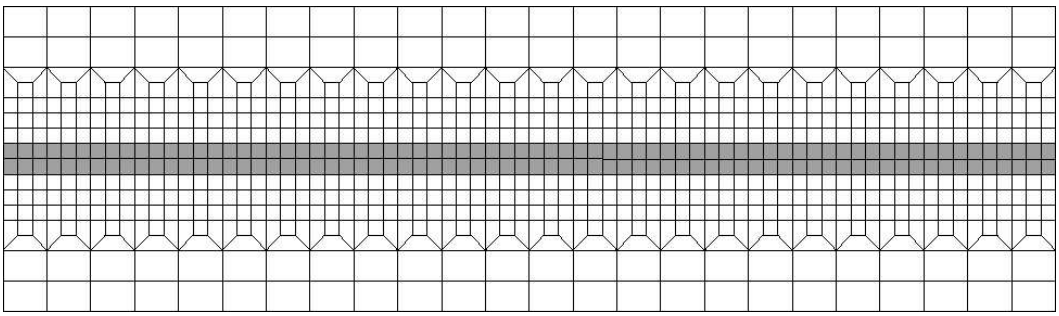

Fig. 4. Soil surface discretization.

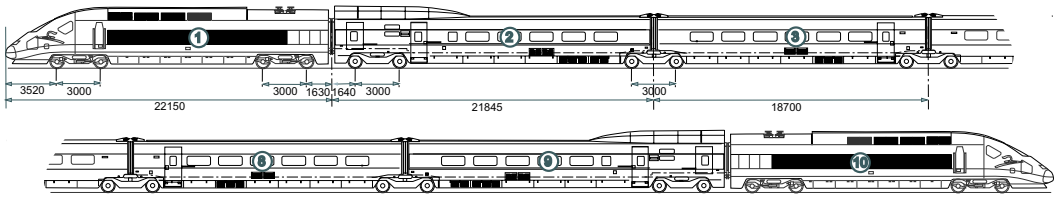

Fig. 5. Configuration of the Alstom (Thalys) high-speed train.

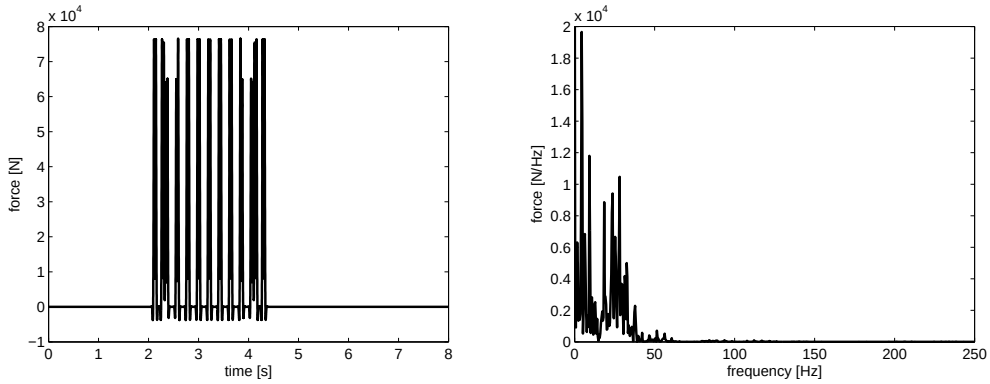

(a) (b)

Fig. 6. Force transmitted by a single sleeper during the passage of a Alstom (Thalys) HST at a speed $v = 315$ km/h: (a) Time history (b) Frequency content.

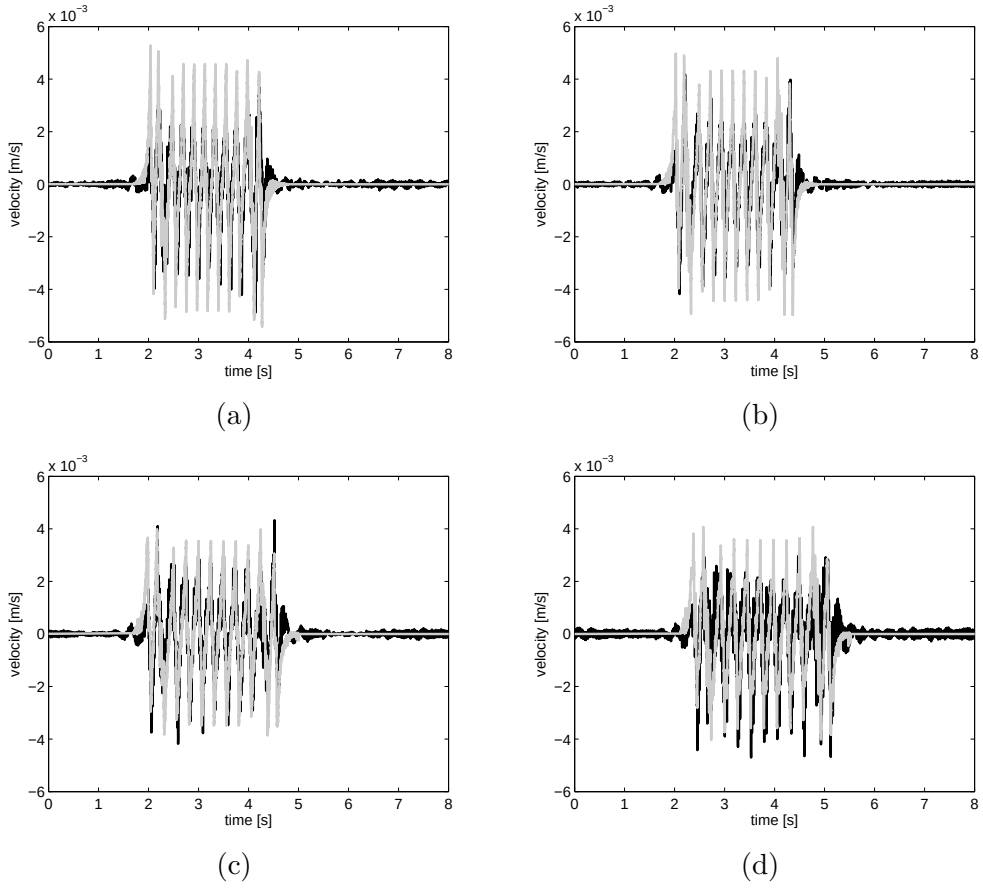

Fig. 7. Vertical velocity at a point 4 m from the track: (a)$v = 315$ km/h (b)$v = 300$ km/h (c)$v = 271$ km/h (d) $v = 256$ km/h. Experimental (black line) vs. Numerical (grey line).

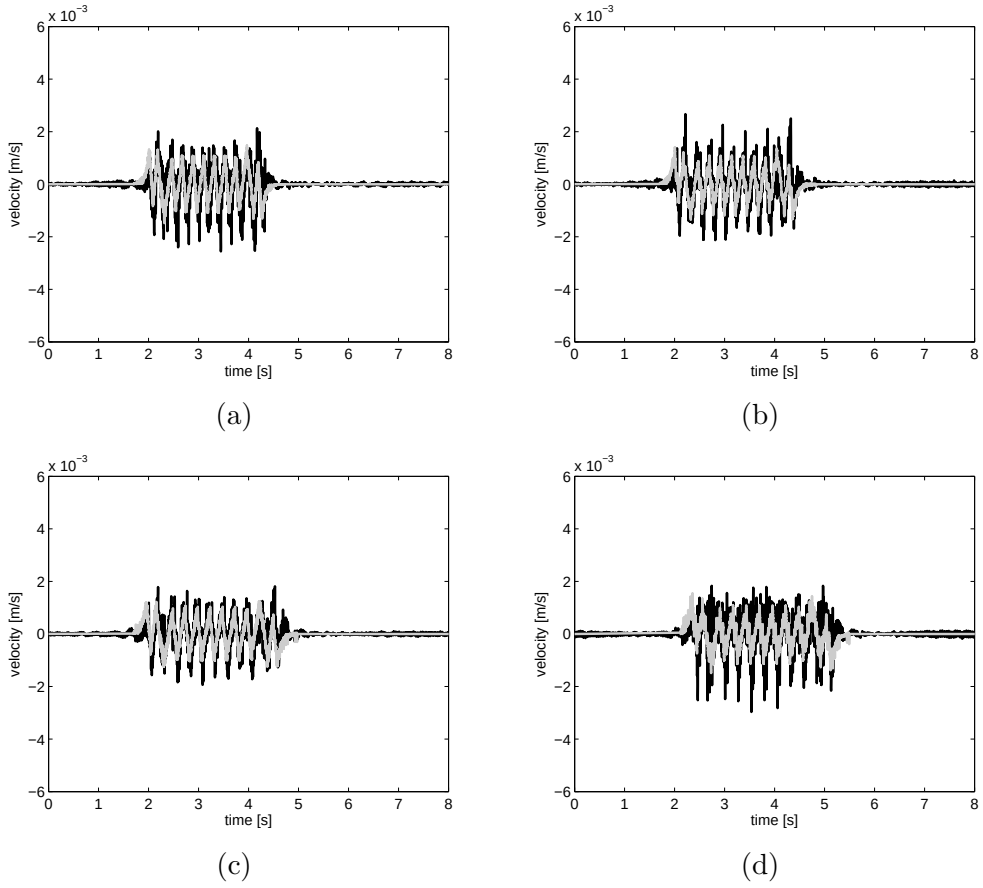

Fig. 8. Vertical velocity at a point 6 m from the track: (a)$v = 315$ km/h (b)$v = 300$ km/h (c)$v = 271$ km/h (d) $v = 256$ km/h. Experimental (black line) vs. Numerical (grey line).

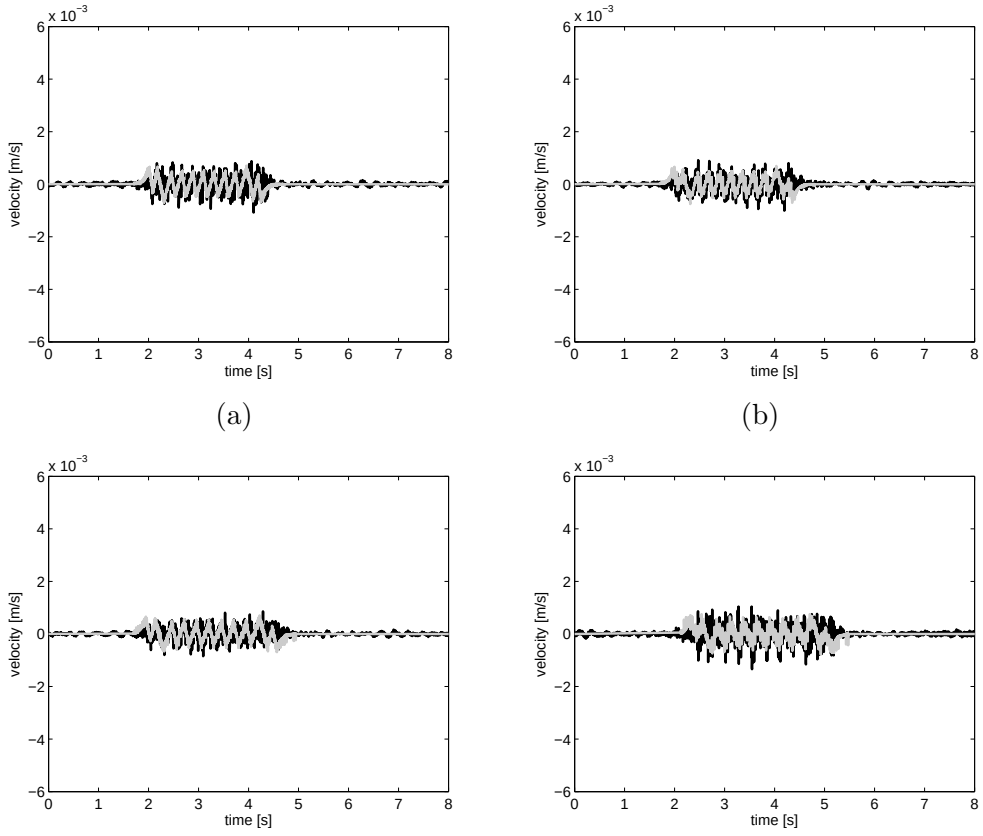

Fig. 9. Vertical velocity at a point 8 m from the track: (a)$v = 315$ km/h (b)$v = 300$ km/h (c)$v = 271$ km/h (d) $v = 256$ km/h. Experimental (black line) vs. Numerical (grey line).

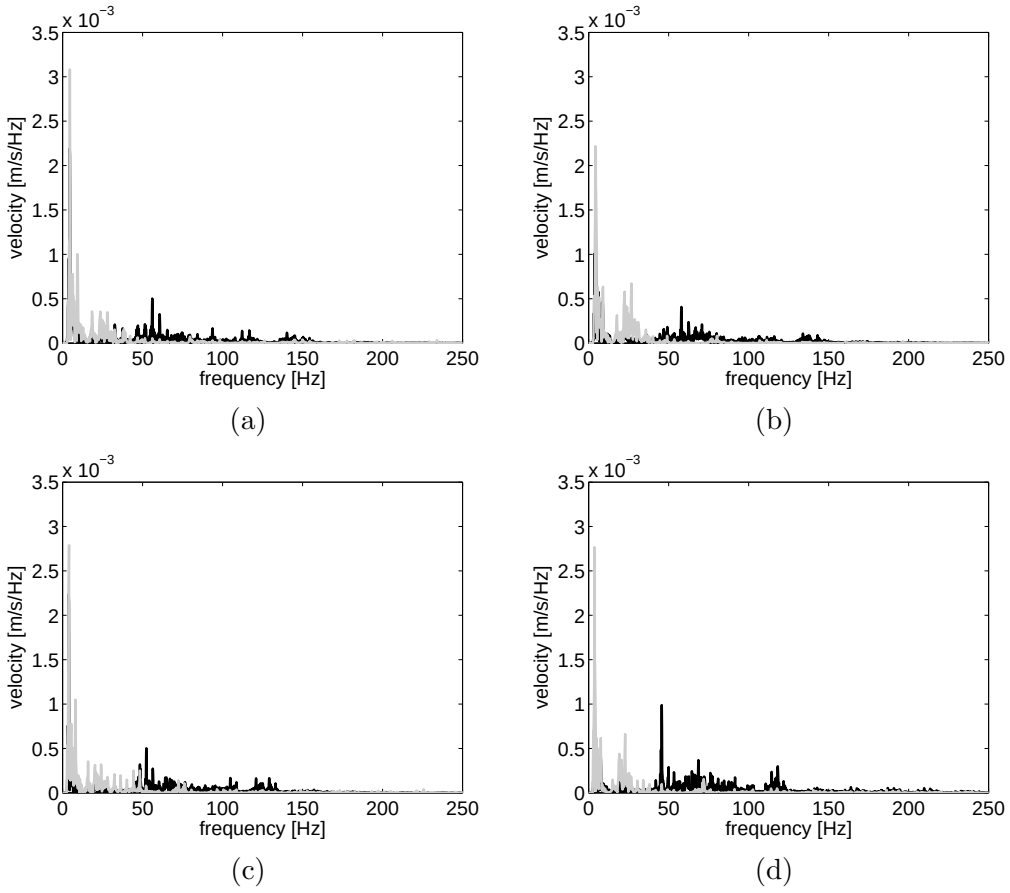

Fig. 10. Frequency content of the vertical velocity at a point 4 m from the track: (a)v = 315 km/h (b)v = 300 km/h (c)v = 271 km/h (d) v = 256 km/h. Experimental (black line) vs. Numerical (grey line).

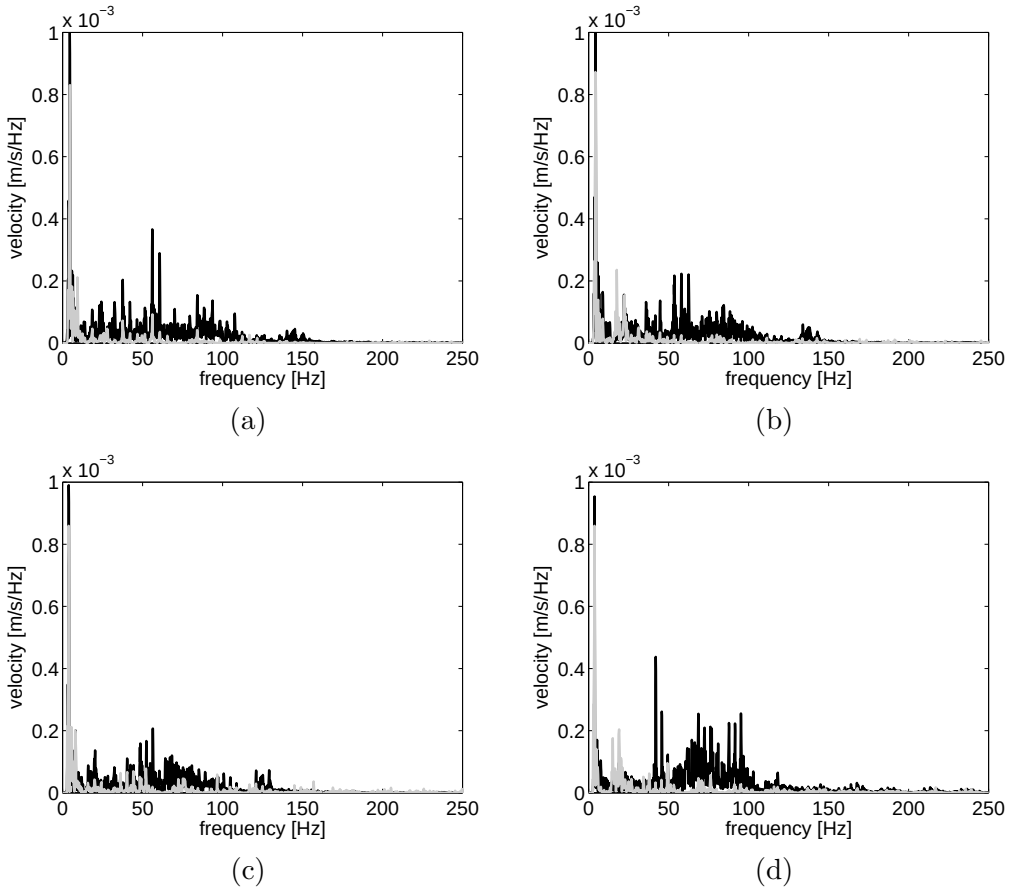

Fig. 11. Frequency content of the vertical velocity at a point 6 m from the track: (a)v = 315 km/h (b)v = 300 km/h (c)v = 271 km/h (d) v = 256 km/h. Experimental (black line) vs. Numerical (grey line).

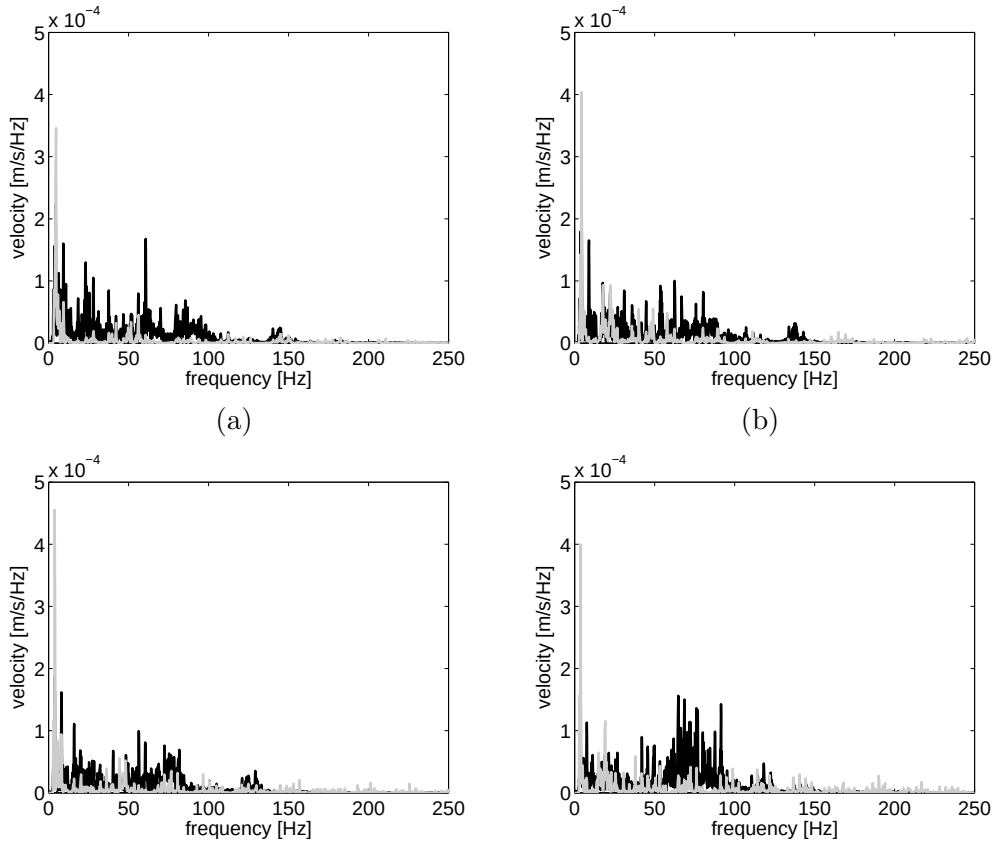

Fig. 12. Frequency content of the vertical velocity at a point 8 m from the track: (a)v = 315 km/h (b)v = 300 km/h (c)v = 271 km/h (d) v = 256 km/h. Experimental (black line) vs. Numerical (grey line).

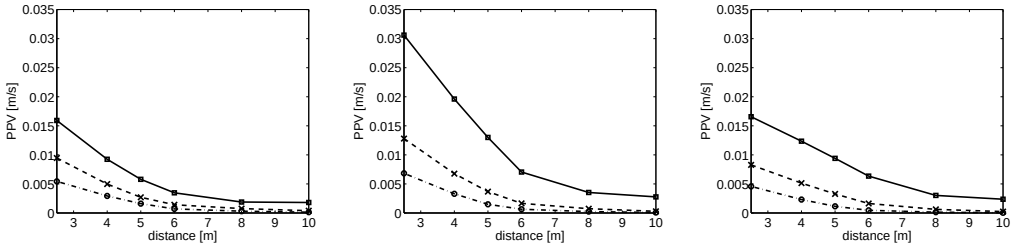

(a) (b) (c)

Fig. 13. Computed PPV as a function of the distance to the track for different damping ratio: '—' $\xi = 0.02$, '– – –' $\xi = 0.04$, '– · –' $\xi = 0.06$. Train speed: (a)$v = 300$ km/h (b)$v = 350$ km/h (c)$v = 500$ km/h.

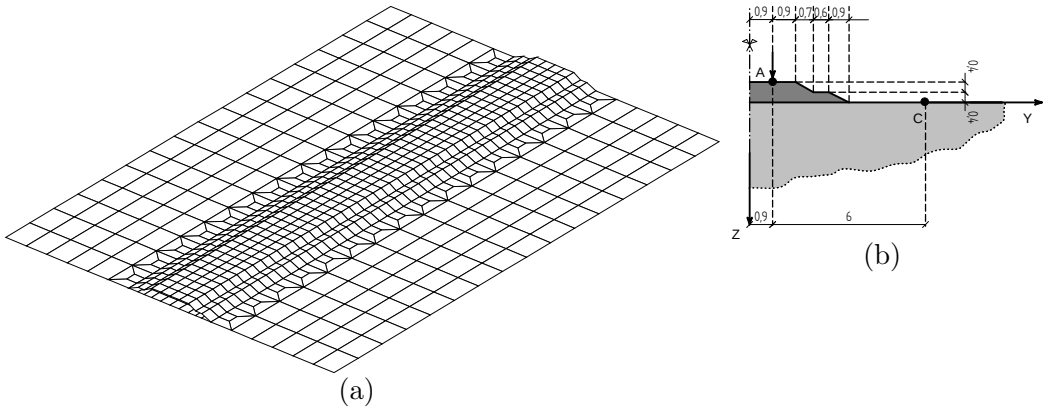

Fig. 14. Half-space with 0.8 m thick ballast embankment. BE discretization and geometry.

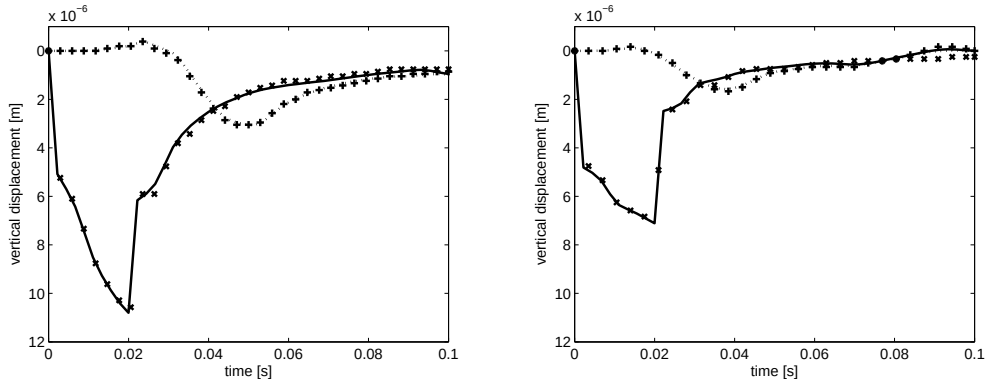

(a) (b)

Fig. 15. Vertical displacements at points A ('–' proposed model vs. '×' Adam et al.) and B ('··' proposed model vs. '+' Adam et al.): (a)Case 1 (b)Case 2.

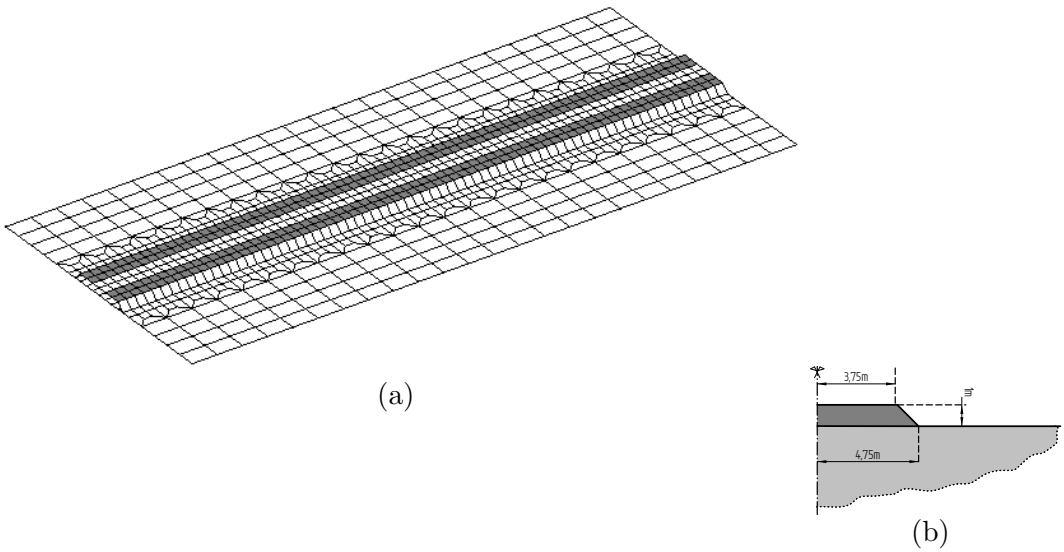

(a) (b)

Fig. 16. Half-space with 1.0 m thick ballast embankment. BE discretization and geometry.

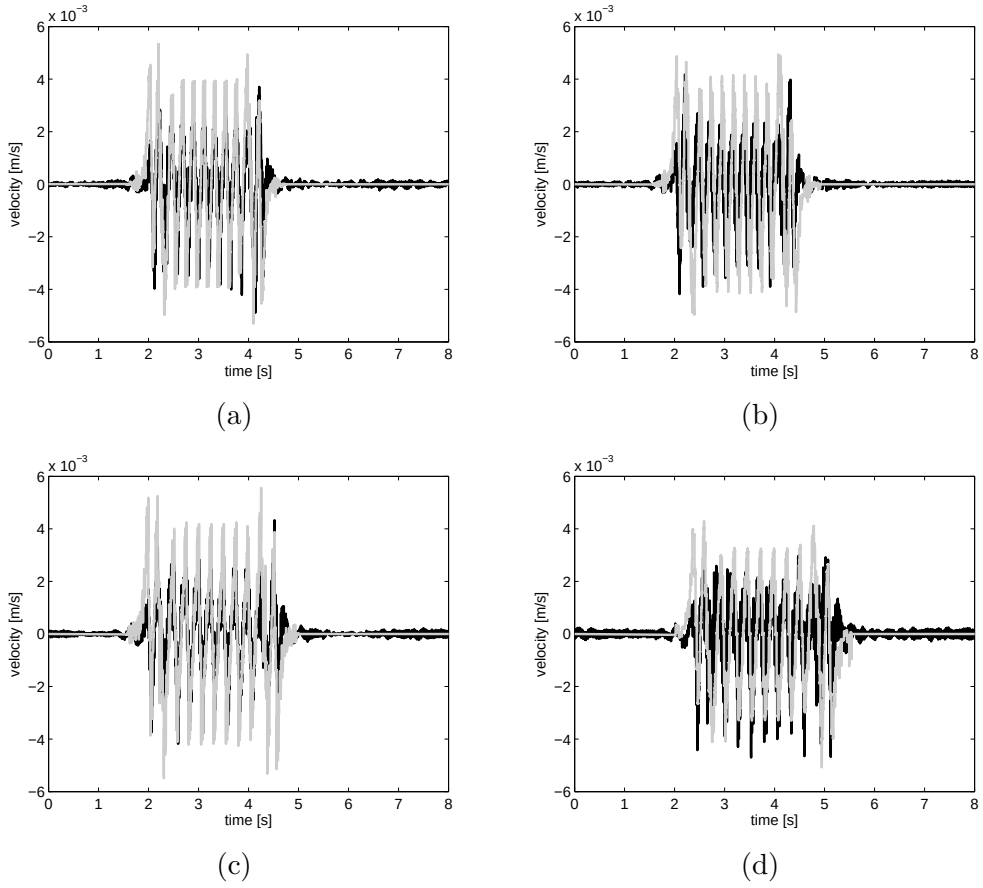

Fig. 17. Vertical velocity at a point 4 m from the track considering a ballast layer: (a)v = 315 km/h (b)v = 300 km/h (c)v = 271 km/h (d) v = 256 km/h. Experimental (black line) vs. Numerical (grey line).

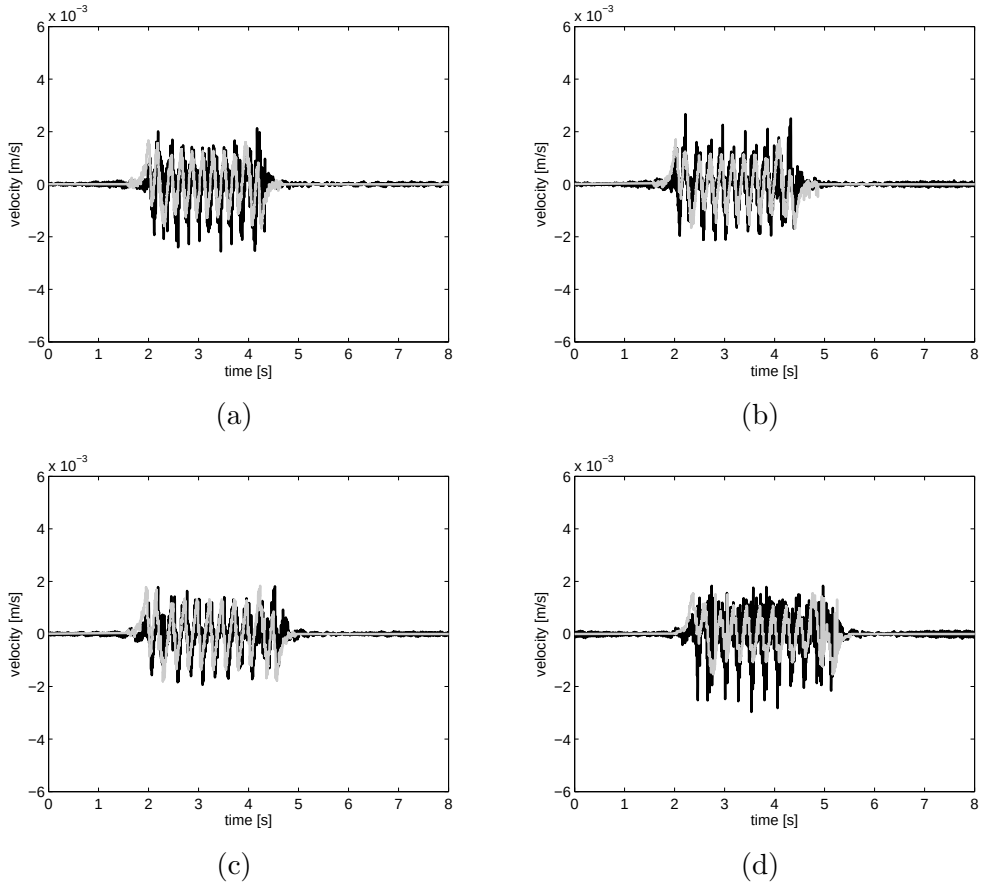

Fig. 18. Vertical velocity at a point 6 m from the track considering a ballast layer: (a)v = 315 km/h (b)v = 300 km/h (c)v = 271 km/h (d) v = 256 km/h. Experimental (black line) vs. Numerical (grey line).

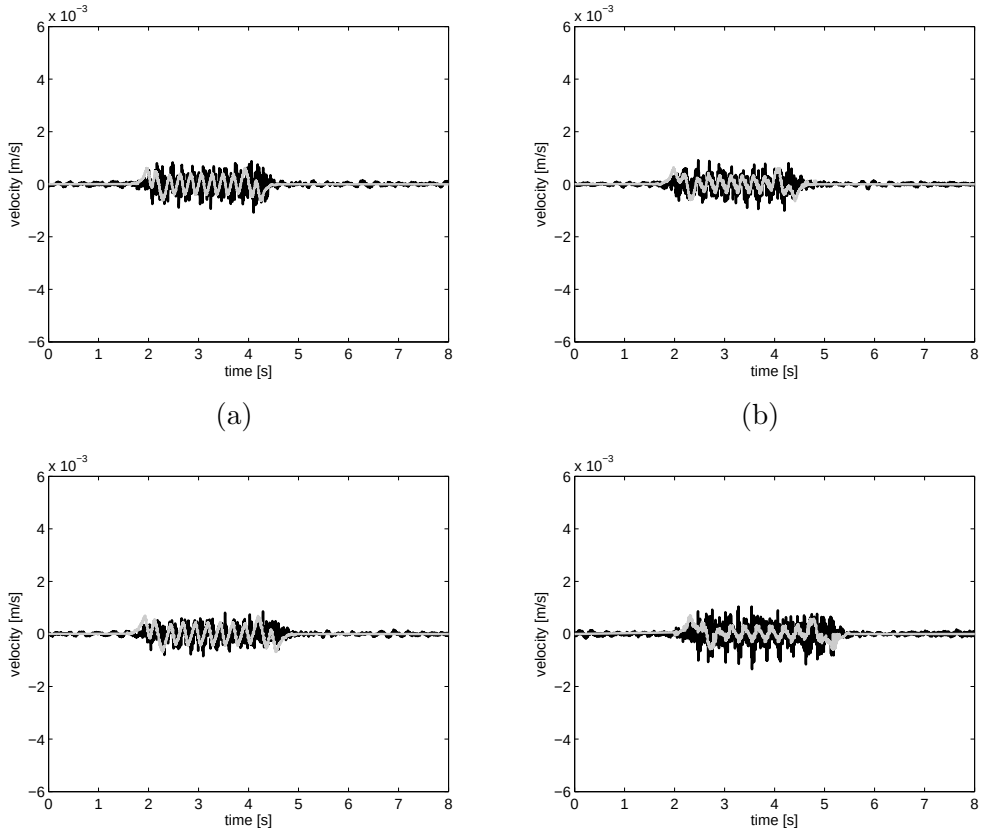

Fig. 19. Vertical velocity at a point 8 m from the track considering a ballast layer: (a)v = 315 km/h (b)v = 300 km/h (c)v = 271 km/h (d) v = 256 km/h. Experimental (black line) vs. Numerical (grey line).

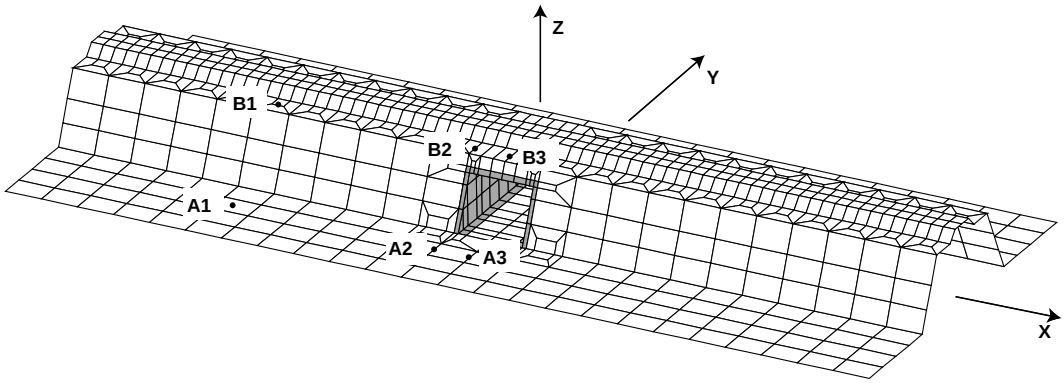

(a)

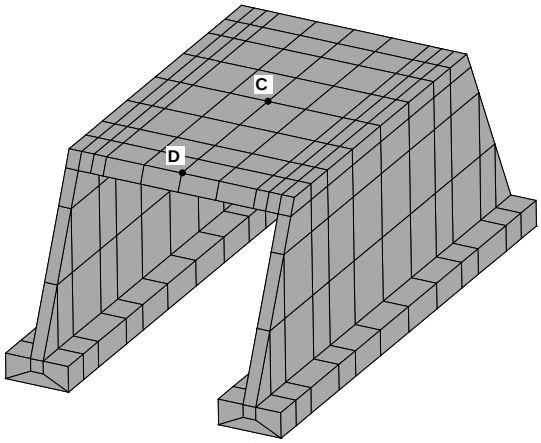

(b)

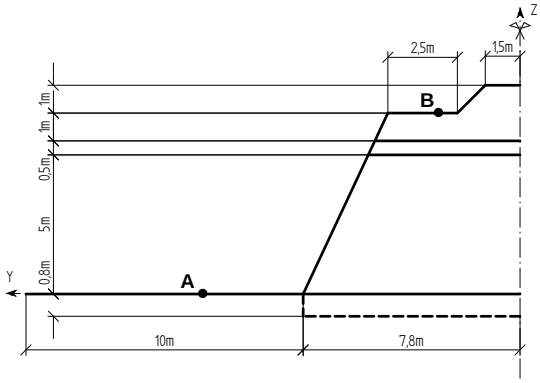

(c)

Fig. 20. Underpass. BE discretization and geometry.

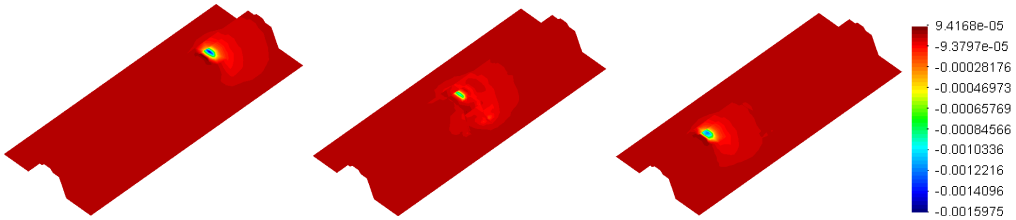

(a) (b) (c)

Fig. 21. Vertical soil surface displacements for the passage of a 15×10^4 N axle with $v = 300$ km/h: (a) $t = 0.267$ s (b) $t = 0.537$ s (c) $t = 0.804$ s.

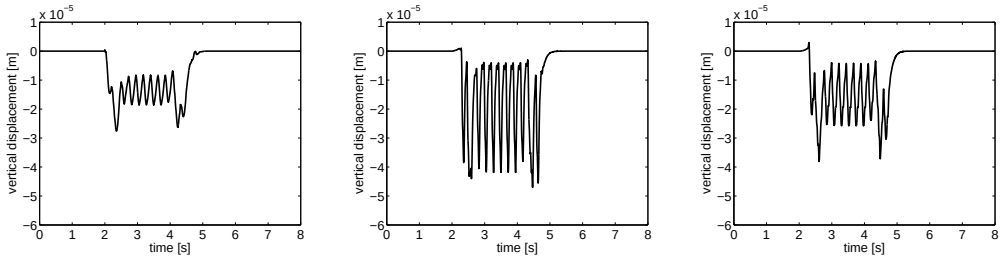

(a) (b) (c)

Fig. 22. Vertical displacement at three points located 11.45 m from the track axis due to the passage of an Alstom (Thalys) HST with $v = 300$ km/h: (a)Point A1 (b)Point A2 (c)Point A3.

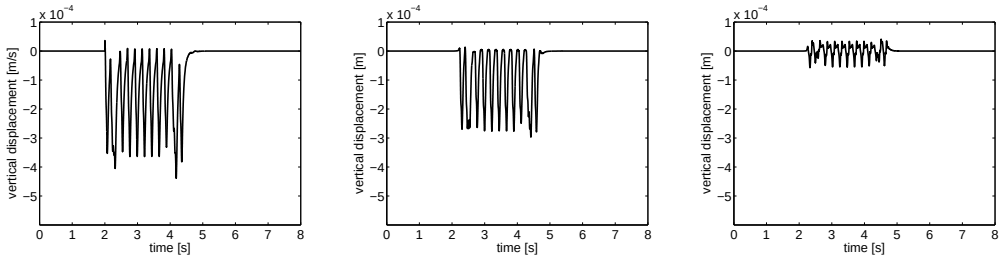

(a) (b) (c)

Fig. 23. Vertical displacement at embankment surface points located 3.60 m from the track axis due to the passage of an Alstom HST with $v = 300$ km/h: (a)Point B1 (b)Point B2 (c)Point B3.

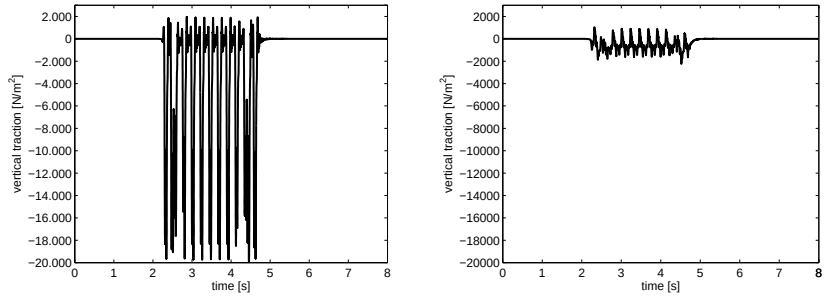

(a) (b)

Fig. 24. Tractions on the underpass deck due to the passage of an Alstom HST with $v = 300$ km/h: (a)Point C (b)Point D.

Table 1: Geometrical and mass characteristics of the Alstom (Thalys) high-speed train

	No. of carriages	No. of axles	$L_t[m]$	$L_b[m]$	$L_a[m]$	$M_t[kg]$
Locomotives	2	4	22.15	14.00	3.00	17000
End carriages	2	3	21.84	18.70	3.00	14500
Central carriages	6	2	10.70	18.70	3.00	17000